Journal of Bio- and Tribo-Corrosion (2019) 5:50
https://doi.org/10.1007/s40735-019-0233-9

Synthesis, Experimental and Theoretical Investigation of Tetrazole Derivative as an Effective Corrosion Inhibitor for Mild Steel in 1 M HCl

H. About[1,2] · M. El Faydy[2] · F. Benhiba[1] · Z. Rouifi[1,2] · M. Boudalia[3] · A. Guenbour[3] · H. Zarrok[1] · B. Lakhrissi[2] · H. Oudda[1] · I. Warad[4] · A. Zarrouk[3]

Received: 18 November 2018 / Revised: 5 March 2019 / Accepted: 7 March 2019 / Published online: 15 April 2019

Abstract
The 2-(4,5-dihydro-4-((8-hydroxyquinolin-5-yl) methyl)tetrazol-1-yl) benzamide, symbolized by QTB is a new organic inhibitor synthesized and characterized using ^{1}H and ^{13}C NMR spectroscopies. The corrosion inhibition of mild steel in 1 M HCl by QTB was studied by gravimetric, electrochemical impedance spectroscopy (EIS) and potentiodynamic polarization methods. The temperature effect on the corrosion behavior of steel in 1 M HCl in the absence and the presence of QTB is studied in the temperature range 298–328 K. Inhibition efficiency of QTB increased with an increase in the concentration of inhibitor and decreased with the increase in temperature. The adsorption of QTB on the steel surface obeys to the Langmuir's adsorption isotherm. The thermodynamic parameters of activation and adsorption were calculated and discussed. The relationship between molecular structure of this compound and their inhibition efficiency has been investigated by ab initio quantum chemical calculations. The Monte Carlo simulation was found to be in good agreement with the experiments.

Keywords Synthesis · Tetrazole derivative · Mild steel · Corrosion inhibition · Adsorption · DFT

1 Introduction

Corrosion is one of the biggest problems encountered by the industrial sector since it used acid as the main solution in the daily processes. The general aggressivity of the acid solutions make it easy for the corrosive attack on the metallic materials [1]. Acid solutions are widely used in industry. The most important areas of application being acid pickling, industrial acid cleaning, acid descaling and oil well acidizing [2].

HCl is generally used in the treatment of steel and ferrous alloys. Because of the general aggression of acid solutions, inhibitors are commonly used to reduce the corrosive attack on metallic materials [3]. Among the alternative corrosion inhibitors, organic compounds containing polar functions with nitrogen, oxygen, or sulfur atoms as well as heterocyclics containing conjugated double bonds have been reported as effective inhibitors of mild steel corrosion in acidic media [4]. The existing data show that most organic inhibitors act by adsorption on the metal surface. This phenomenon is influenced by the nature and surface charge of metal, by the type of aggressive electrolyte and by the chemical structure of inhibitors [5].

Quantum chemical calculations may supplement the experimental studies or even predict with confidence some experimentally unknown properties. Density functional theory (DFT) in particular, has been applied to analyze the characteristics of the inhibitor/surface mechanism and to determined the electronic structure and reactivity of the molecule in corrosion inhibition studies [6].

Up to now, many *N*-heterocyclic compounds such as pyrimidine derivatives [7], the tetrazole derivatives [8],

Electronic supplementary material The online version of this article (https://doi.org/10.1007/s40735-019-0233-9) contains supplementary material, which is available to authorized users.

✉ A. Zarrouk
azarrouk@gmail.com

[1] Laboratory of Separation Processes, Faculty of Science, IbnTofail University, Kenitra, Morocco

[2] Laboratory of Agro-Resources, Polymers and Process Engineering, Department of Chemistry, Faculty of Science, IbnTofail University, PO Box 133, 14000 Kenitra, Morocco

[3] Laboratory of Materials, Nanotechnology and Environment, Faculty of Sciences, Mohammed V University, Av. Ibn Battouta, Agdal, Box 1014, Rabat, Morocco

[4] Department of Chemistry, AN-Najah National University, P.O. Box 7, Nablus, Palestine

triazole derivatives [9] were used for the corrosion inhibition of iron or steel in acidic media. The quinoline derivatives are one of the important constituents of pharmacologically active synthetic compounds [10], including biological activities [11]. Accordingly, the aim of this paper is to study the inhibiting action of a new organic compound containing 8-hydroxyquinoline. The electrochemical behaviour of mild steel in HCl media in the absence and presence of inhibitor namely QTB have been studied by potentiodynamic polarization, electrochemical impedance spectroscopy techniques and gravimetric methods. The effect of temperature (298–328 K) on corrosion and inhibition processes are thoroughly assessed and discussed. Thermodynamic parameters governing the adsorption process were also calculated and discussed. Theoretical calculations were performed using using DFT and Monte Carlo simulations and correlated with the inhibiting effect of QTB.

2 Experimental Details

2.1 Synthesis of Inhibitor QTB

The synthesis of 2-(4,5-dihydro-4-((8-hydroxyquinolin-5-yl)methyl)tetrazol-1-yl) benzamide (QTB) is described according to the following reaction (Scheme 1). Acetic acid was added with stirring to a suspension of 2-aminobenzamide (5×10^{-3} mol), and 5-azidomethyl-8-quinolinol (1 g, 5×10^{-3} mol) in triethylorthoformate (5×10^{-3} mol), and the mixture was refluxed for 12 h. The progress of the reaction was monitored by TLC using hexane–acetone (4:6, v/v) as eluent. The mixture was neutralized by NaOH addition solution and then it was extracted with dichloromethane. The organic phase was recovered and dried over anhydrous $MgSO_4$ and then evaporated. The residue obtained was purified by silica gel column chromatography with *n*-hexane–acetone mixture (6:4, v/v) as the mobile phase, to give 2-(4,5-dihydro-4-((8-hydroxyquinolin-5-yl)methyl)tetrazol-1-yl) benzamide (QTB).

The structure of the (QTB) was confirmed by ^{1}H NMR and ^{13}C NMR spectra.

^{1}H NMR (300 MHz, Me_2SO-d_6), δppm = 6.533–8.835 (m, 10H, quinoline and benzamide), 3.948 (s, 2H, quinoline-CH_2-tetrazol), 4.655(s, 2H, –CH_2 of tetrazol).

^{13}C NMR (300 MHz, Me_2SO-d_6), δ_{ppm} = 53.097 (quinoline-CH_2-tetrazol); 111.321, 127.838, 128.950, 133.777, 119.954, 120.341, 122.291, 138.042, 148.372 (CH-quinoline and aniline); 127.918, 139.672, 128.950, 129.304, 136.373, 152.740, (C-quinoline and aniline); 86.423 (–CH_2–tetrazol), 168.926 (C=O).

The ^{1}H NMR, ^{13}C NMR spectra are attached in supplementary data.

2.2 Solutions

The acid solutions (1 M HCl) were prepared by dilution of analytical grade 37% HCl with distilled water. The concentration range of the used 2-(4,5-dihydro-4-((8-hydroxyquinolin-5-yl)methyl)tetrazol-1-yl) benzamide (QTB) was 10^{-6} to 10^{-3} M, it is noted that the studied organic product is highly soluble in dimethyl sulfoxide (DMSO).

2.3 Gravimetric and Electrochemical Measurements

Gravimetric measurements were carried out in a double-walled glass cell equipped with a thermostated cooling condenser. The mild steel specimen used in this study had a rectangular form (1.5 cm × 1.5 cm × 0.3 cm) with a chemical composition (in wt%) of 0.370% C, 0.230% Si, 0.680% Mn, 0.016% S, 0.077% Cr, 0.011% Ti, 0.059% Ni, 0.009% Co, 0.160% Cu and the remainder iron (Fe) were used for electrochemical and gravimetric studies. The surface of the test electrode was mechanically abraded by different grades of emery papers with 220 up to 1200, rinsed with distilled water, cleaned with acetone and finally dried at hot temperatures. Then, the loss in weight was determined by analytic balance after 6 h of immersion at 298 K. Triplicate experiments were performed in each case and the mean value of the weight loss was calculated.

Scheme 1 Synthesis of the compound QTB

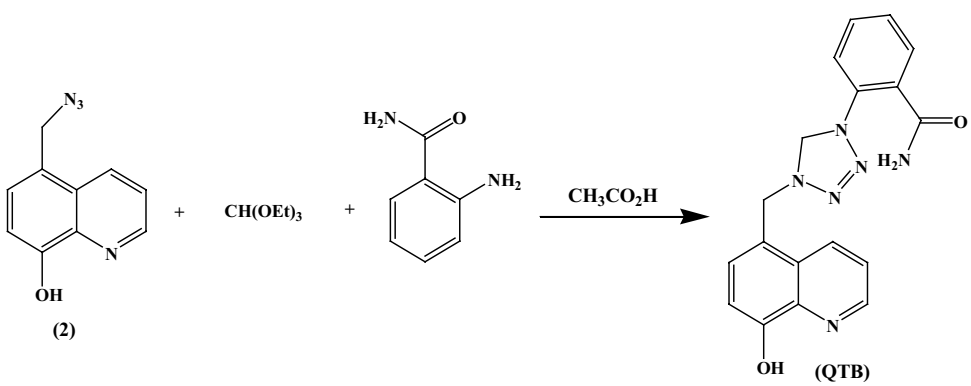

Electrochemical experiments were conducted using an electrochemical measurement system Tacussel Radiometer PGZ 100 controlled by a PC supported by Voltamaster 4 Software. The potentiodynamic polarization curves and electrochemical impedance spectroscopy (EIS) were carried out in a standard three-electrode cell. The saturated calomel electrode (SCE) and the platinum electrode were used as reference and auxiliary electrode, respectively, while the mild steel specimen was used as working electrode in an exposed surface area of 1 cm^2. Before starting the experiments, the working electrode was immersed in test solutions for 30 min to attain a steady state open circuit potential (*E*ocp). After measuring of *E*ocp, the electrochemical measurements were performed. The potential was swept to anodic potentials by a constant sweep rate of 0.5 mV s^{-1} and potential was scanned in the range of − 800 to − 200 mV/SCE relative to the corrosion potential. The impedance diagrams are given in the Nyquist representation. The electrochemical impedance spectroscopy (EIS) measurements were performed with a frequency range of 100 kHz to 10 mHz and amplitude of 5 mV with 10 points per decade.

2.4 Quantum Chemical Calculations

Quantum chemical calculations were performed by density functional theory (DFT) level with the non-local correlation functional B3LYP, combining Becke's three-parameter exchange functional with the correlation functional of Lee et al. at basis sets 6-31G(d,p) [12, 13].The following quantum chemical parameters were considered: the energy of the lowest unoccupied molecular orbital (E_{LUMO}), the energy of the highest occupied molecular orbital (E_{HOMO}), energy band gap $\Delta E = E_{HOMO} - E_{LUMO}$, the electron affinity (A), the ionization potential (I) and the number of transferred electrons (ΔN).

2.5 Monte Carlo Simulations

Monte Carlo simulations were carried out to model the mode of adsorption of the investigated inhibitor molecule on Fe(110) surface. The adsorption locator code implemented in the Material Studio (MS) 8.0 software was adopted in this simulation. Fe(110) crystal surface was selected for this simulation and to represent MS because it is the most stable surface [14]. The condensed phase optimized molecular potentials for atomistic simulation studies (COMPASS) force field was used for the simulation of all molecules and systems [15]. The simulation of the corrosion inhibitor molecule designated as QTB on Fe(110) surface was carried out to locate the low-energy adsorption sites of the potential corrosion inhibitors on Fe surface.

3 Results and Discussion

3.1 Weight Loss Measurements

The corrosion of mild steel in 1 M HCl medium of QTB at 298 K was studied by weight loss measurements. The corrosion parameters obtained by conducting weight loss measurements for mild steel in the absence and presence of different concentration of QTB in 1 M HCl after 6 h of immersion at 298 K are given in Table 1.

From the weight loss results, the inhibition efficiency $\eta_\omega(\%)$ was calculated using Eq. 1:

$$\eta_\omega(\%) = \frac{C_R - C_{R(\text{inh})}}{C_R} \times 100 \quad (1)$$

where C_R and $C_{R(\text{inh})}$ represent the corrosion rates in the absence and presence of the inhibitor in HCl solution and θ is the degree of surface coverage of the inhibitor. The values of percentage inhibition efficiency and corrosion rate obtained from weight loss method at different concentrations at 298 K are summarized in Table 1.

It has been observed that the inhibition efficiency of this compound increases with the increase in concentration attain 85.1% for 10^{-3} M. This increase can be attributed to the adsorption of this compound at the mild steel/acid solution interface. The height inhibitions of the studied triazole is may be due to the interactions between the π electrons of the aromatic systems and unshared electrons pairs of the heteroatoms (− N, − O) which form a bond with the vacant 3*d* orbitals of the metal surface leading to the formation of a protective film.

3.2 Potentiodynamic Polarization Measurements

Figure 1 shows current–potential characteristics resulting from cathodic and anodic polarization curves of steel in 1 M HCl without and with various concentrations of the synthesized inhibitor (from 1×10^{-6} to 1×10^{-3} M) at 298 K. The electrochemical parameters such as corrosion current (i_{corr}), corrosion potential (E_{corr}), cathodic Tafel slope (β_c) for QTB obtained from polarization measurements are listed

Table 1 Gravimetric results of mild steel in 1 M HCl without and with addition of QTB at 298 K

Medium	Conc. (M)	C_R (mg cm^{-2} h^{-1})	η_w (%)
HCl	1	0.429 ± 0.008	–
QTB	10^{-6}	0.137 ± 0.009	68.1
	10^{-5}	0.109 ± 0.008	74.6
	10^{-4}	0.085 ± 0.002	80.2
	10^{-3}	0.064 ± 0.008	85.1

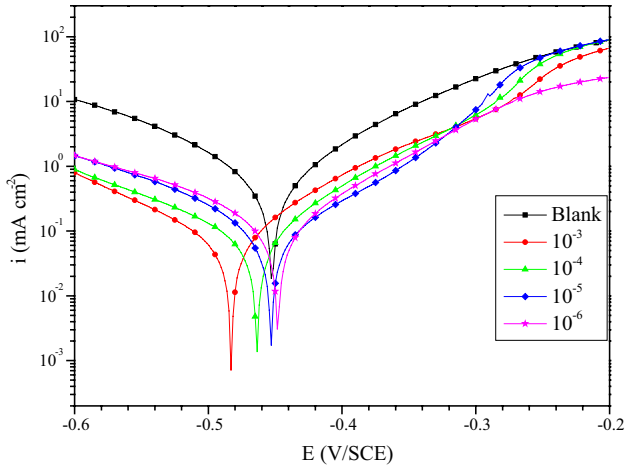

Fig. 1 Polarization curves for mild steel in 1 M HCl containing different concentrations of QTB at 298 K

in Table 2. However, the electrochemical parameters such as corrosion current density (i_{corr}), corrosion potential (E_{corr}) and cathodic Tafel slope (β_c) obtained by curve fitting using the following equation:

$$i = i_a + i_c = i_{corr}\{\exp\left[b_a \times (E - E_{corr})\right] - \exp\left[b_c \times (E - E_{corr})\right]\} \quad (2)$$

where i_{corr} is the corrosion current density ($A\ cm^{-2}$), b_a and b_c are the Tafel constants of anodic and cathodic reactions (V^{-1}), respectively. These constants are linked to the Tafel slopes β (V/dec) in usually logarithmic scale given by Eq. (3):

$$\beta = \frac{\ln 10}{b} = \frac{2.303}{b} \quad (3)$$

The inhibition efficiency was evaluated from the measured i_{corr} values using the following relationship:

$$\eta_{PP}(\%) = \frac{i^0_{corr} - i_{corr}}{i^0_{corr}} \times 100 \quad (4)$$

where i^0_{corr} and i_{corr} are the corrosion current densities for mild steel electrode in the uninhibited and inhibited solutions, respectively.

The Table 2 shows an increase in inhibition efficiency, while the corrosion current density decreased with increasing of the inhibitor concentration. This may be due to the adsorption of inhibitor on mild steel/acid interface. Clearly, i_{corr} decreased remarkably while η_{pp} increased with the increasing of the inhibitor concentration, and the maximum (η_{pp}) is up to 89.3% at 10^{-3} M of inhibitor. There is no definite trend in the shift of E_{corr} in the presence of corrosion inhibitor, therefore, the synthesized inhibitor can be arranged as a mixed-type inhibitor, and the inhibitory action is caused by the geometric blocking effect [16]. Namely, the inhibitory action comes from the reduction of the reaction area on the surface of the corroding metal. From the polarization curves, it was noted that the curves were shifted toward lower current density region. However, the cathodic Tafel slopes (β_c) change with the QTB addition suggesting that studied molecule was first adsorbed onto the electrode surface and impeded by merely blocking the reaction sites of the steel surface without affecting the cathodic reaction.

3.3 Electrochemical Impedance Spectroscopy

The corrosion-inhibiting properties of QTB on mild steel was also investigated by electrochemical impedance spectroscopy (EIS). Figures 2a and 3 represented as Nyquist and Bode-phase plots, respectively, show the impedance spectra for mild steel corrosion in HCl solution with and without various concentrations of QTB. In all the studied frequency range, the Nyquist plots (Fig. 2a) show single semicircles which correspond to one time constant in Bode plots. Inspection of Fig. 2a revealed that the increasing of QTB concentration increases the size of the capacitive loop. (Figure 2a). This increase is linked to the adsorption of inhibitor molecules on the metal inteface. Generally, this type of diagram indicates that the corrosion reaction is controlled by transfer charges process on a heterogeneous and irregular solid surface electrode [17]. The depressed capacitive loops at the higher frequencies is usually linked to the frequency dispersion also to inhomogeneities, mass transport process and roughness of steel surface [18].

However, impedance behavior can be explained using a simple equivalent circuit (Fig. 2b) composed of the solution resistance (R_s), charge transfer resistance (R_{ct}) and constant phase element (CPE) were calculated and summarized in

Table 2 Electrochemical polarization parameters for corrosion of mild steel in 1 M HCl with different concentrations of QTB at 298 K

C_{inh} (M)	$-E_{corr}$ (mV/SCE)	$-\beta_c$ (mV dec^{-1})	i_{corr} (μA cm^{-2})	η_{PP} (%)
Blank solution	454.4	101.1	590	–
10^{-6}	451.0	109.2	106	81.7
10^{-5}	457.8	87.5	72	87.6
10^{-4}	468.0	112.0	66	88.6
10^{-3}	487.3	106.5	63	89.3

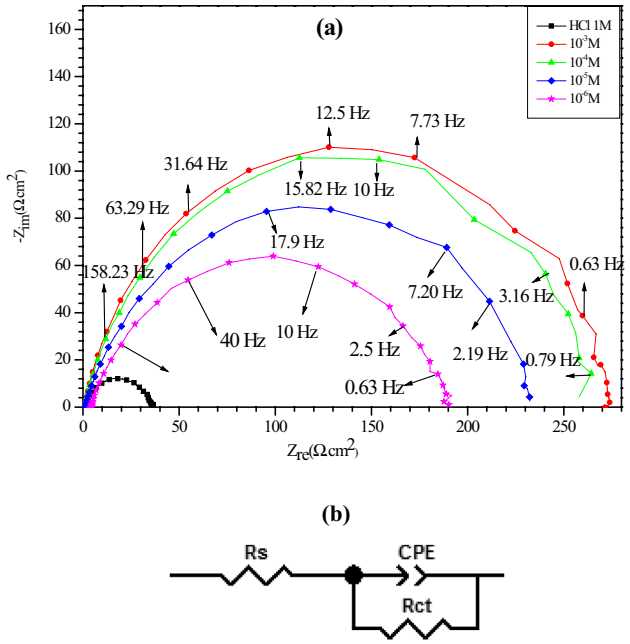

Fig. 2 **a**The Nyquist plots of mild steel in 1 M HCl containing various concentrations of synthesized compound at 298 K and **b** the Equivalent electrochemical circuit for fitting of the results

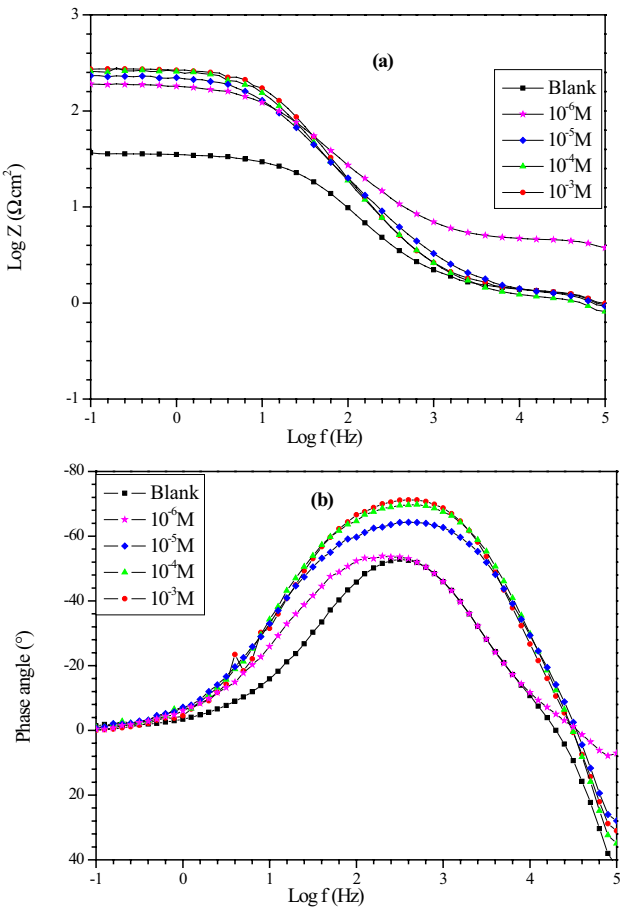

Fig. 3 Bode plots (**a**) and phase angle (**b**) for mild steel in 1 M HCl in the absence and presence of different concentrations of QTB

Table. The use of CPE to obtain more accurate study of impedance behavior of the electric double layer, CPE was used as the alternative for capacitor and which expressed by foloweiy equation

$$Z_{CPE} = A^{-1}(iw)^{-n} \tag{5}$$

where A is the CPE constant, n is the CPE exponent (ranges from 0 to 1), $i^2 = -1$ is an imaginary number and w is the angular frequency.

However, The double layer usually (C_{dl}) behaves as a constant phase element (CPE) when the value of n is equal to unity, the C_{dl} values are obtained by exploiting the next formula (5) [42]:

$$C_{dl} = \left(AR_{ct}^{1-n}\right)^{1/n} \tag{6}$$

The protection efficiency obtained from the charge transfer resistance is calculated using the following equation:

$$\eta_z = \frac{R_{ct}^{i} - R_{ct}^{0}}{R_{ct}^{i}} \times 100 \tag{7}$$

where, and R_{ct}^{0} and R_{ct}^{i} are the charge transfer resistance in absence and in presence of inhibitor, respectively.

The Bode diagrams have two levels: the first at high frequency is attributed to the resistance of the electrolyte R_s and the second at low frequency is attributed to the charge transfer resistor R_{ct}. The module of the impedance |Z| low frequency that is related to the charge transfer resistance increases with the increase in the concentration of inhibitor, this shows that the inhibitory power of this compound increases with the increase in concentration that can be attributed to the adsorption of inhibitor molecules on the surface of steel.

Table 3 indicate that the charge transfer resistance R_{ct} values increased and the double-layer capacitance C_{dl} values decreased with increasing inhibitor concentration. The inhibition efficiency values (η_z%) increases with the inhibitor concentrations to reach a maximum of 88.14% at 10^{-3} M. The increase in R_{ct} value can be attributed to the formation of protective film on the metal/solution interface. However, it should be noted that the value of the proportional factor A of CPE changed in a regular manner way with QBT concentrations. The increase of the values of n when compared with 1 M HCl and with concentration can be linked to some decrease of the surface heterogeneity, due to the adsorption of the QBT molecules on the active adsorption sites whereas, the decrease in the C_{dl} values may be caused by a decrease in the local dielectric constant and/or an increase

Table 3 Electrochemical data for mild steel in 1 M HCl in the absence and presence of different concentrations of QTB at 298 K

Medium	C_{inh} (M)	R_s (Ω cm^2)	R_{ct} (Ω cm^2)	CPE		C_{dl} (μF cm^{-2})	η_z (%)
				10^5 A (Ω^{-1} S^n cm^2)	n		
1 M HCl	00	1.439 ± 0.03	32.00 ± 0.04	70.12 ± 0.006	0.840 ± 0.002	272.66	–
QTP	10^{-6}	1.230 ± 0.05	183.1 ± 0.08	43.35 ± 0.008	0.868 ± 0.005	97.81	82.52
	10^{-5}	1.231 ± 0.04	229.4 ± 0.02	32.32 ± 0.009	0.870 ± 0.003	68.37	86.05
	10^{-4}	1.121 ± 0.04	260.0 ± 0.01	20.94 ± 0.006	0.875 ± 0.009	37.06	87.69
	10^{-3}	1.160 ± 0.04	270.0 ± 0.03	13.03 ± 0.007	0.880 ± 0.001	19.06	88.14

in the thickness of the electrical double layer, indicating that the inhibitors function by adsorption at the metal surface [19, 20].

3.4 Effect of Solution Temperature

The influence of temperature on the inhibition performance of QTB for mild steel in 1 M HCl electrolyte was examined by potentiodynamic polarization measurements (Fig. 4) and the extracted parameters are listed in Table 4.

From results given in Table 4, a modification of corrosion potential with increase in temperature. Whereas, the inhibition efficiency decreased with increasing temperature as a result of the higher dissolution of mild steel at higher temperature, which might cause the desorption of QTB from the mild steel surface [21].

The activation parameters of the corrosion process were calculated at the different temperatures, without and with QTB. In addition, the activation energy (E_a) was determined using the i_{corr} values obtained from the potentiodynamic polarization curves, according to equation [22]:

$$i_{corr} = k\,exp\left(-\frac{E_a}{RT}\right) \tag{8}$$

An alternative formula of the Arrhenius equation which can determine the activation enthalpy (ΔH_a) and entropy (ΔS_a) using the following equation:

$$i_{corr} = \frac{RT}{Nh}\exp\left(\frac{\Delta S_a}{R}\right)\exp\left(\frac{\Delta H_a}{RT}\right) \tag{9}$$

where i_{corr} is the corrosion current density, h is the Planck's constant, N is the Avogadro number, R is the universal gas constant, E_a is the activation energy for the corrosion process, k is the Arrhenius pre-exponential constant and T is the absolute temperature [23].

Figure 5 present the variation of the corrosion current density logarithm as a function of the absolute temperature inverse. A straight lines are obtained with regression coefficients close to unity.

Figure 6 shows a plot of Ln (i_{corr}/T) vs. 1/T. Straight lines are obtained with a slope of ΔH_a/R and an intercept of Ln (R/Nh + ΔS_a /R) from which the values of ΔS_a and ΔH_a are calculated.

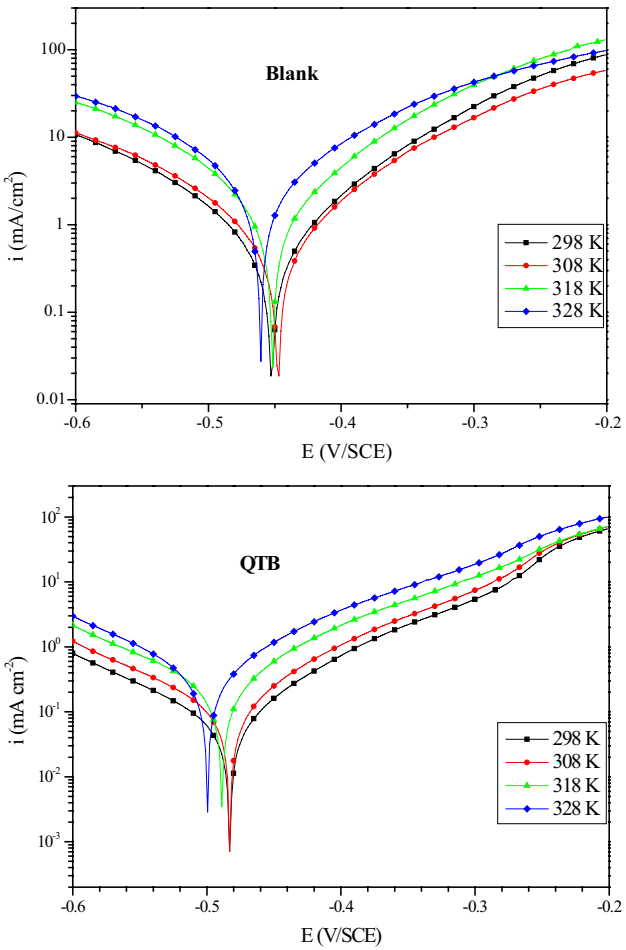

Fig. 4 Polarization curves for mild steel in 1 M HCl without and with 10^{-3} M of QTB at different temperatures

The addition of QTB leads to an increase in the apparent activation energy E_a from 37.64 to 47.61 kJ mol^{-1} which indicates that the dissolution of mild steel in HCl electrolyte in the presence of synthesized compound is lower than the free electrolyte. This increase probably was attributed to physisorption of QBT on the steel surface [24, 25]. However, the enthalpy value is greater in the presence of QBT

Table 4 Electrochemical parameters of mild steel in 1 M HCl without and with optimum concentration of QTB at different temperatures

Medium	T (K)	E_{corr} (mV/SCE)	$-\beta_c$ (mV dec^{-1})	i_{corr} (μA cm^{-2})	η_{PP} (%)
1 M HCl	298	−454.4	101.1	590	–
	308	−451.1	104.9	820	–
	318	−454.8	111.1	1324	–
	328	−464.3	101	2368	–
QTB	298	−487.3	106.5	64	89.1
	308	−487.6	112.3	107	86.9
	318	−493.4	113.4	203	84.6
	328	−503.7	110.5	365	84.5

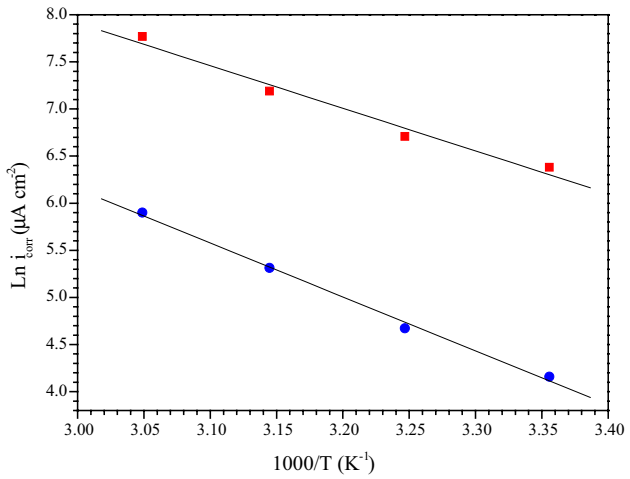

Fig. 5 Ln i_{corr} vs. 1/T for mild steel in 1 M HCl in the without and with optimum concentration of QTB

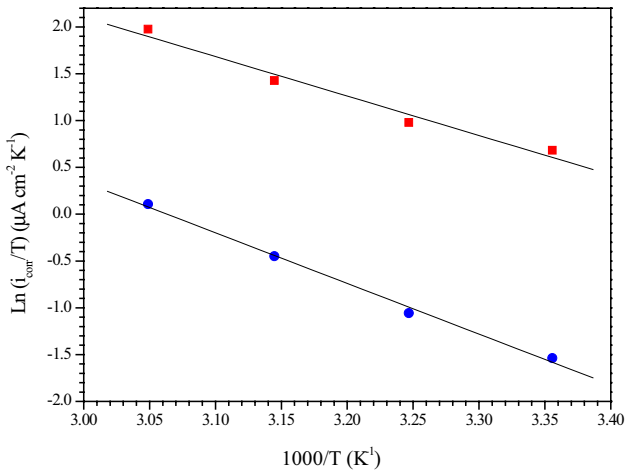

Fig. 6 Ln (i_{corr}/T) versus 1000/T for mild steel in 1 M HCl solution in the absence and presence of synthesized compound

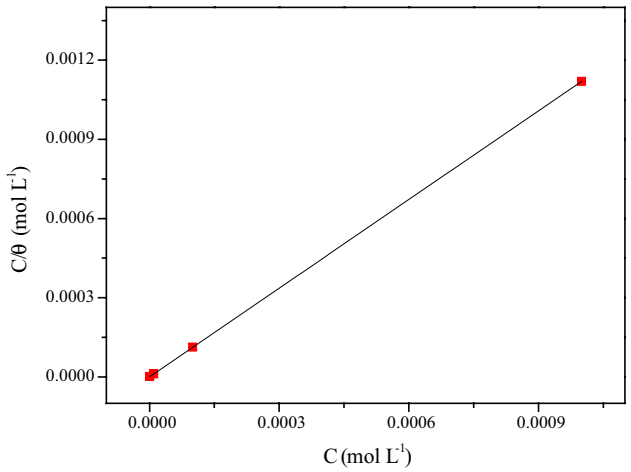

Fig. 7 Langmuir adsorption isotherm of QTB on mild steel surface in 1 M HCl at 298 K

(45.01 kJ mol^{-1}) than in its absence (35.04 kJ mol^{-1}). The positive sign of enthalpy reflects the endothermic nature of the dissolution process. Moreover, the large negative value of ΔS_a (−59.78 J mol^{-1} K^{-1}) implies that there is decrease in the disorder during the transformation of the reactants into complex [26].

3.5 Adsorption Isotherm

To evaluate the adsorption process of phytochemical organic compound on the steel surface, adsorption isotherms are employed to describe the adsorption process. Among different adsorption isotherms, the Langmuir adsorption isotherm is the most fundamental so was tested at first. The correlation between θ and QTB concentration can be studied by Eq. 10.

$$\frac{C}{\theta} = \frac{1}{K} + C \tag{10}$$

where K is the equilibrium constant of the adsorption process and θ (η_{pp}/100) is the fraction of metal surface covered by the QTB. The variation plot of C/θ versus C (Fig. 7) gives straight lines with a correlation coefficient close to unity suggesting that the adsorption of QTB on the mild steel surface obeyed a Langmuir adsorption isotherm [27–30]. The

Table 5 Adsorption parameters of QTB for mild steel corrosion in 1 M HCl

	Slope	R^2	K (L mol^{-1})	ΔG°_{ads} (KJ mol^{-1})
QTB	1.1	1.0	2510853.16	−46.46

value of equilibrium constant (K) was calculated from the interception of the straight line in Fig. 7. The equilibrium constant is related to the standard-free energy of adsorption (ΔG°_{ads}) by the following equation (Eq. 11):

$$\Delta G^{\circ}_{ads} = -RT \ln(55.5\ \mathrm{K}) \tag{11}$$

where the 55.5 in the above formula is the concentration of water.

Generally, the standard-free energy of adsorption values of −20 kJ mol^{-1} or less negative are associated with an electrostatic interaction between charged molecules and charged metal surface (physisorption); those around −40 kJ mol^{-1} or higher involve charge sharing or transfer from the inhibitor molecules to the metal surface to form a coordinate covalent bond (chemisorption). The considered ΔG°_{ads} value as delineated in Table 5 is lower than −40 kJ mol^{-1} which implies that the absorption process is of the chemisorption nature [31].

3.6 Quantum Chemical Calculation

3.6.1 Optimization, Distribution of the Electronic Density and Calculation of the Main Quantum Parameters of Compound QTB

The DFT theory is a very important method for studying the reactivity of inhibitory molecules [32]. In this sense, we will follow a well structured procedure using several very precise descriptors. The first factor is the densities HOMO and LUMO; this is shown in Fig. 8 with the electrostatic contour and the optimized molecule of QTB. According to this figure, it is clear that the electron density HOMO is located on the entire molecular surface of QTB, while the LUMO density is distributed around the aromatic cycles of quinoline.

The values of the E_{HOMO} and E_{LUMO} energies are calculated using DFT based on Beck's three-parameter exchange functional and Lee–Yang–Parr nonlocal correlation functional (B3LYP) and the 6–31 G* orbital basis sets for all atoms as implemented in Gaussian 09 program [33, 34]. From these values, we can extract the different parameters' structural quantum of compound QTB such as ΔEgap ($E_{LUMO} - E_{HOMO}$), the dipole moment (μ), the total electronegativity (χ), the overall hardness (η), the chemical softness (σ), electrophile index (ω), nucleophile index (ε), and the number of electrons transferred from the inhibitor to the surface of the metal (ΔN_{110}); these parameters are tabulated in Table 6.

The results of the table shows that the high value of E_{HOMO} (−4.807 eV) and the low value of E_{LUMO} (−1.405 eV) reflect that the ability to give and accept the molecule electrons studied is very important, respectively. This indicates that the adsorption capacity of this inhibitor QTB on the metal surface increases with the variation of these energies. Concerning the number of electrons transferred (ΔN_{110}), if the value of $\Delta N_{110} < 3.6$, the inhibitory performance of a molecule has increased with the increase of the electron donating capacity of this molecule to the metal surface [35, 36]. The number of electron transfer (ΔN) was calculated using the following equation [37]:

$$\Delta N = \frac{\chi_{Fe} - \chi_{inh}}{2(\eta_{Fe} + \eta_{inh})} \tag{12}$$

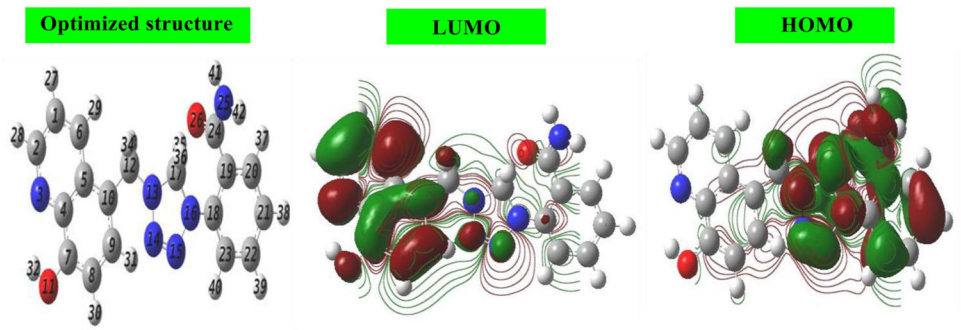

Fig. 8 Optimized structure, HOMO and LUMO of QTB molecule

Table 6 Calculated quantum parameters of QTB inhibitor

Parameter	E_{LUMO} (eV)	E_{HOMO} (eV)	ΔE_{gap} (eV)	μ (D)	η (eV)	σ (e V^{-1})	χ (eV)	ω	ε	ΔN_{110}
QTB	−1.405	−4.807	3.402	7.208	1.702	0.587	3.106	1.417	0.705	0.504

where χ_{Fe} and χ_{inh} denote the absolute electronegativity of iron and the inhibitor molecule, respectively, and η_{Fe} and η_{inh} denote the absolute hardness of iron and the inhibitor molecule, respectively. The values of χ_{Fe} and η_{Fe} are taken as 7 eV mol^{-1} and 0 eV mol^{-1}, [38, 39] respectively.

In that case, the value of ΔN_{110} is also recorded in Table 6; it shows that the inhibitory power resulting from electron donation is in very good agreement with the Lukovit study [12]. The consequence of this behavior facilitates the transfer of electrons between the test molecule and the electrode surface.

This finding suggests that the inhibition efficiency increases with increasing softness and decreases on increasing the hardness of the inhibitor molecules. Absolute electronegativity (χ), global hardness (η) and global softness (σ) are estimated using the equations [40, 41].

$$\chi = \frac{I + A}{2} \tag{13}$$

$$\eta = \frac{I - A}{2} \tag{14}$$

$$\sigma = \frac{1}{\eta} = -\frac{2}{E_{HOMO} - E_{LUMO}} \tag{15}$$

The ionization potential (I) and the electron affinity (A) are defined as follows equations:

$$I = -E_{HOMO} \tag{16}$$

$$A = -E_{LUMO} \tag{17}$$

From Table 6, we observed that the high values of χ_{inh} and η_{inh} indicate that our inhibitor is very reactive with the metal surface of iron.

On the other hand, to measure the ability to accept electrons from a molecule we used the electrophilicity index (ω). On the other side, the nucleophilicity index (ε) is another element for measuring the electron donating power of this molecule. Therefore, a molecule with a lower value of ε and a higher value of ω is considered a good corrosion inhibitor [42].

$$\omega_{inh} = \frac{\chi_{inh}^2}{2\eta_{inh}} \tag{18}$$

$$\varepsilon_{inh} = \frac{1}{\omega_{inh}} \tag{19}$$

From Table 6, it is well noted that the electrophilicity and nucleophilicity agree with the experimental results.

3.6.2 Active Sites of the QTB Molecule

When an organic molecule carries several atoms and heteroatoms either as donors or acceptors of electrons, it is considered as an effective inhibitor against corrosion [43]. For this purpose, we used well-known methods such as the Mulliken atomic charges, the total electronic densities mapped and the Fukui indices (FI). Fig. 9 represents the Mulliken atomic charge distribution of QTB. The representation of the atomic charges of the inhibitory molecule QTB shows that atoms carrying negative charges are considered as electron donor sites (nucleophiles) lorsqu'ils interagissent avec la surface du fer pour former des liaisons de coordination. Therefore, Fig. 9 shows that oxygen, nitrogen and some carbon atoms carry more negative charges according to the following sequence: N3, C10, O11, C12, N13, N14 and N15 while the carbon atoms C2, C4, C7, C17, C18 and C24 contain a high density of positive charges. This indicates that these atoms play a role as active sites accepting electrons from iron orbitals to form bonds of retro-donation. In parallel, the total electronic densities mapped are also shown in Fig. 9. The strong electron density is represented by a red color and the low electron density is represented by a blue color [44–46]. The high electron density (yellow to red color) is delocalized around the oxygen atom of the hydroxy group which is directly related to the quinoline family of QTB, this could be easily attributed to free doublets of

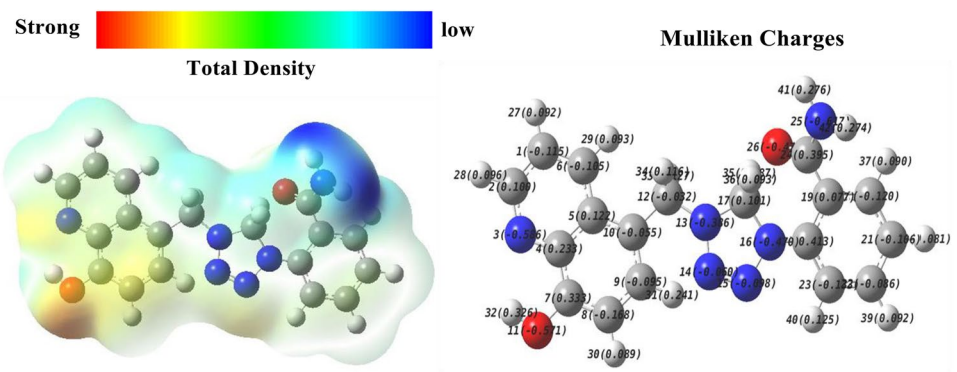

Fig. 9 Distribution of the total electron density mapped and the Mulliken atomic charges of the QTB molecule

electrons on this atom. Contrarily, the low electron density presented by green and blue colors is located on some carbon and nitrogen atoms and. Thus, atoms have strong electronic densities. They could be good candidates for adsorbing on the surface of Fe (low electron density).

The Fukui index (IF) is the third parameter which describes a local reactivity of an inhibitory molecule. This method allows us to distinguish the different functional groups responsible for nucleophilic and/or electrophilic attacks [47, 48]. These are determined, respectively, by the maximum values of f_k^+ and f_k^-. Such that a high value of f_k^+ measures the electron density variations when a molecule has received an additional electron and f_k^- measure the electron density when a molecule loses electron [49, 50]. Table 7 collates the various calculated values of Fukui indices. These parameters are shown in Fig. 10.

Analysis of the results obtained in Table 7 and Fig. 10 shows that the QTB molecule has the highest values of f_k^+, these last ones are localized on the atoms. N13, N14, N15 and N16. These cities can be accepted electrons while the highest values of f_k^- shows that atoms N13, C6 and O31 are able to give electrons which leads to the increase of QTB compound adsorption capacity on the metal surface.

We conclude that the results obtained by the local reactivity (IF) study confirm the results obtained by the total electron density and the Mulliken atomic charge.

Table 7 Calculated Fukui indices of QTB molecule using GGA/BOP function with DNP (3.5) base

Atomes	f_k^+	f_k^-
C1	0.027	0.009
C2	0.048	0.008
N3	**0.098**	0.012
C4	0.015	0.005
C5	−0.010	0.007
C6	**0.108**	−0.006
C7	0.041	0.013
C8	0.037	0.004
C9	0.032	−0.003
C10	0.047	−0.015
O11	**0.055**	0.020
C12	−0.009	−0.027
N13	−0.012	**0.075**
N14	−0.021	**0.088**
N15	0.025	**0.061**
N16	−0.003	**0.077**
C17	−0.003	−0.026
C18	−0.003	−0.006
C19	0.002	0.038
C20	0.002	0.013
C21	0.010	0.047
C22	0.010	0.010
C23	0.001	0.036
C24	−0.003	−0.002
N25	0.005	0.020
O26	0.003	0.017

The values in bold are the most significant

3.6.3 Protonation Effect on the Quantum Parameters of QTB

The QTB compound has several active sites available for protonation, but in this work we chose the two N3 and N14 nitrogen atoms as shown in Fig. 11 as the two most favorable sites for protonation. Our chosen based on several factors, On the one hand the molecular electrostatic potential and the effective atomic charge of Mulliken and on the other hand the proton affinity (PA). The latter is a very important descriptor for determining the chemical reactivity of a molecule. Indeed, the molecule that has this lower descriptor, so it is more reactive (Table 8).

PA is calculated from the total energies of the compound studies according to the following equation:

$$\mathrm{PA} = E_T(\text{Inhibitor protoned}) - E_T(\text{Inhibitor}) - E_T\left(H_3O^+\right) + E_T\left(H_2O\right) \quad (20)$$

To determine the site and/or sites most favorable for protonation for the two protonated nitrogen atoms (N3 and N14) we did several protonation tests each time, we protonate an atom, and in the end the protonation is done both at the same time.

The results are shown in Fig. 12. The latter shows that the weak mapped electronic density presented by a blue color (positive region) is localized on the entire molecular surface of QTB and well condensed on the protonated atoms. The main values of the chemical quantum parameters of the protonated and unprotonated studied molecule are recorded in Table 8.

The analysis of Table 8 shows that after the protonation of QTB molecule in the different sites of the nitrogen atoms, the E_{HOMO} values of QTB compound are shifted to values which are more negative than the E_{HOMO} values of QTB neutral.

This indicates that the protonated forms of compound studied have an ability to accept electrons higher than the neutral form [47]. Whereas, the electron donor capacity (ΔN_{110}) of protonated QTB was decreased and negative compared to the unprotonated form, this means that donating electrons from the inhibitory molecule to the metal surface is no longer possible [46]. These results probably show that the interaction between these protonated inhibitors and the surface of the iron is electrostatic in nature.

The proton affinity of molecule is a necessary parameter to measure its basicity. According to this theory, the

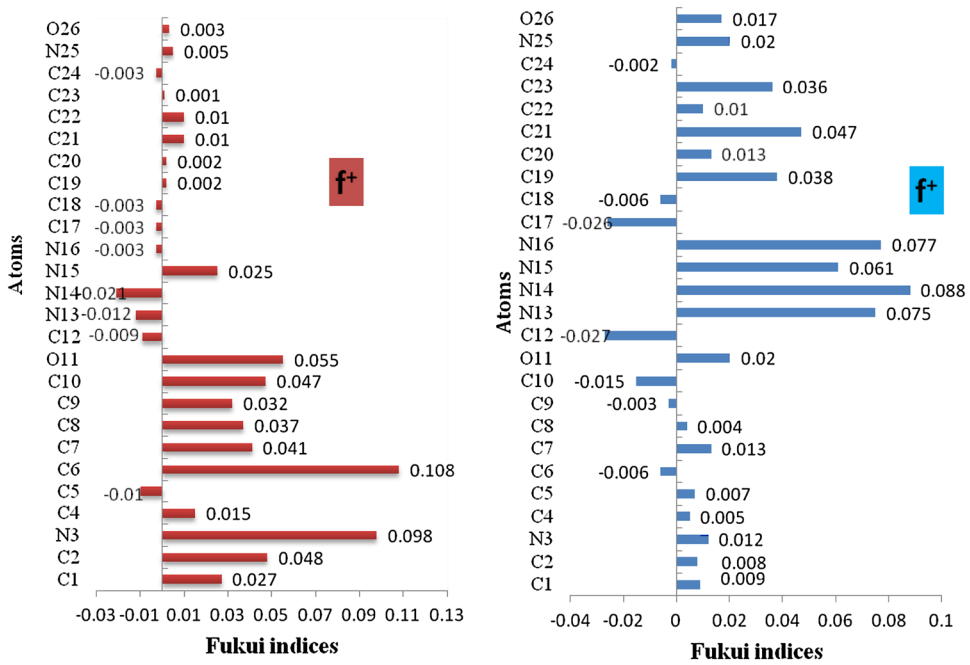

Fig. 10 Bar graphs of Fukui indices of the molecule studied

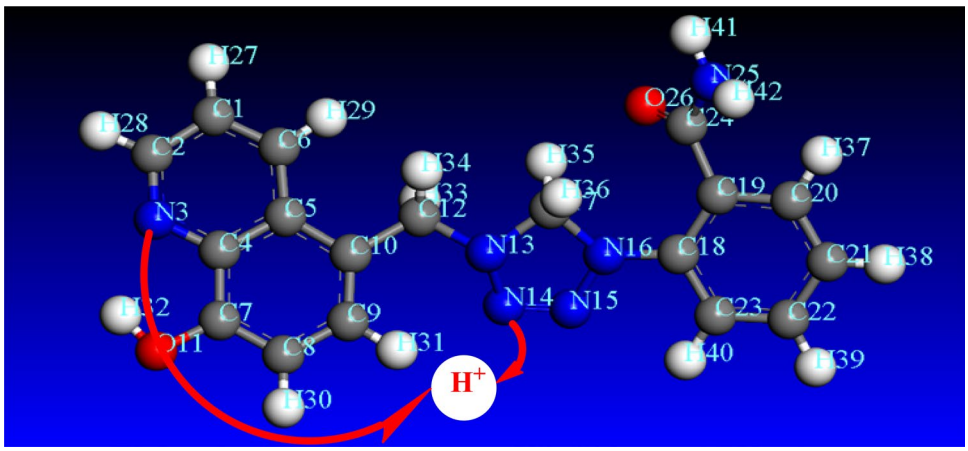

Fig. 11 Atoms available for the protonation of the QTB molecule

Table 8 Main values of the quantum parameters of the protonated and unprotonated QTB molecule

Formrs	PA (Kcal/mol)	E_{LUMO} (eV)	E_{HOMO} (eV)	ΔE_{gap} (eV)	ΔN_{110} (eV)	ET (u a)
QTB (neutre)	–	−1.405	−4.807	3.402	0.504	−1174.27
QTB (N3) H^+	−543.423	−6.051	−7.973	1.922	−1.140	−1174.86
QTB (N14) H^+	−537.148	−5.989	−8.408	2.419	−0.983	−1174.85
QTB (N3N14) H^{2+}	−725.401	−8.819	−12.394	3.575	−1.113	−1175.15

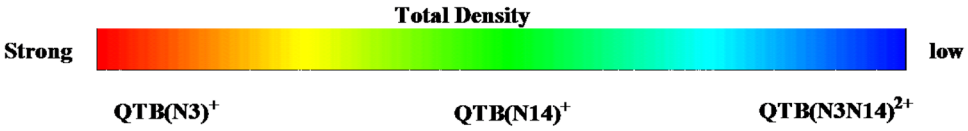

Fig. 12 Electrostatic property of the protonated QTB molecule

Lewis acids and bases are described in terms of electron pair transfers. A Lewis base is an electron pair donor and indeed, Les inhibiteurs de corrosion sont des bases de Lewis [50]. It should be noted that the value of proton affinity increases negatively which leads to its inhibitory efficiency also increasing. PA values are also listed in Table 8, the comparison between the different PA values of the protonated molecule QTB shows that the double protonation of the nitrogen atoms leads to the decrease in the AP value; this indicates that the chemical reactivity increases of protonated QTB and sorted in the following order:

$$PA\left(QTB\left(N_3N_{14}\right)H^{2+}\right) > PA\left(QTB\left(N_3\right)H^{+}\right) > PA\left(QTB\left(N_{14}\right)H^{2+}\right)$$

3.7 Monte Carlo (MC) Simulations of the QTB Molecule

To understand the mechanism and the mode of action of a molecule on a metal surface we performed the simulation by the Monte Carlo method. The study of the adsorption behavior of the QTB molecule on the surface Fe(110) in the gaseous and aqueous phase. The inhibitory molecule QTB was optimized before being placed on the surface of the Fe(110). Figure 13 shows the energy curve according to the optimization steps of QTB in neutral and isolated form using the DMol^3/m-GGA/BOP/DNP basic set.

Figure 13 shows that the inhibitory molecule QTB has an optimal energy of (− 1174.175 Ha), Corresponding stability of QTB in neutral forms. The adsorption energy distribution for the Fe (110)/(QTB) system obtained by the adsorption localization module is shown in Fig. 14. The latter shows that the adsorption energy of the QTB molecule reaches (− 51.0 kcal mol^{-1}) this value is considered as the suitable adsorption energy on the metal surface of Fe(110).

The values of total energy, average total energy, Van der Waals energy, electrostatic energy and intermolecular energy for QTB/iron systems have been calculated by optimizing

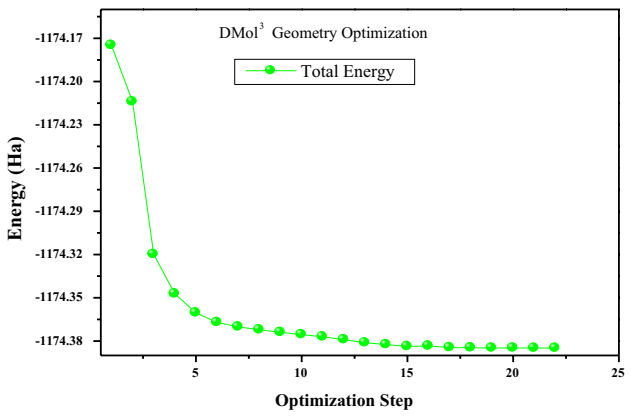

Fig. 13 Energy optimization of neutral QTB molecule using DMol3/m-GGA/BOP/DNP

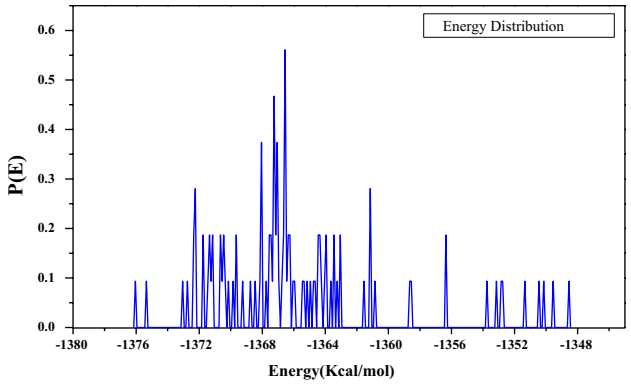

Fig. 14 Adsorption energy distribution for Fe(110)/(QTB) system using adsorption locator module

the whole systems and the total adsorption energy distribution is shown in Fig. 15 for the system under study.

The MC simulation reasonably predicts the most favorable configuration of the adsorbed inhibitor on the metal surface. In this context, side and top views of stable adsorption configurations for QTB on Fe(110) are shown in Fig. 16. It is well noted that the inhibitory molecule has been adsorbed parallel (plane) on the studied surface. In addition, this molecule QTB covers a larger area of coverage towards a metal dissolution block. Whereas, the observation of Fig. 16 shows that the absolute distance between the inhibitor QTB and the surface of the Fe(110) is < 3.6 Å, this indicates that the adsorption nature is chemical type.

The binding energy ($E_{binding}$) is calculated by the following equation:

$$E_{binding} = -E_{int} \tag{21}$$

In other words, it can be said that a greater value of $E_{binding}$ shows that the molecule is absorbed more easily on

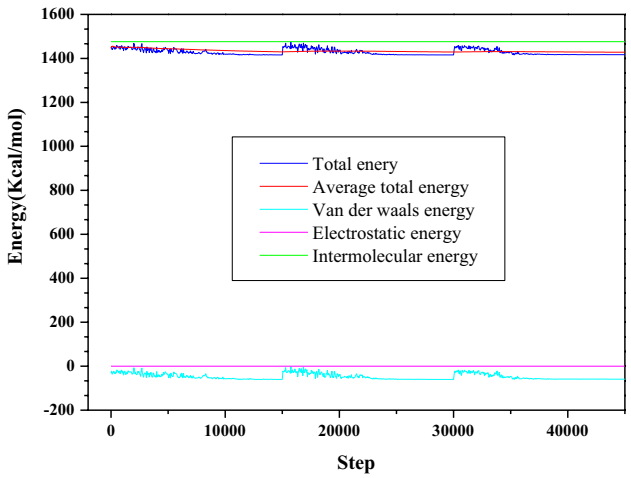

Fig. 15 Total energy distribution for QTB/Fe(110) surface

the metal surface studied and that inhibitory performance is higher spontaneously [51]. From Table 9, the calculated interaction energy values (E_{int}) for QTB is − 1376.030 kcal/mol.

Figure 17 shows the minimum and maximum values of the force field for the Fe(110)/QTB interface. The iso-surface colors change to reflect the minimum and maximum values associated with the field which has been mapped on the total electronic density.

Greater dot density means more likely adsorption sites of the inhibitor molecule QTB on the Fe(110) metal surface.

4 Conclusion

A new organic compound namely 2-(4,5-dihydro-4-((8-hydroxyquinolin-5-yl)methyl)tetrazol-1-yl) benzamide (QTB) was synthesized and characterized using ^{1}H and ^{13}C NMR spectroscopies. The corrosion inhibition of mild steel in 1.0 M HCl by QTB was studied using experimental and theoretical techniques. The temperature effect on the corrosion behaviour of steel in 1 M HCl in the absence and the presence of QTB is studied in the temperature range 298–328 K. Inhibition efficiency increases with increase in

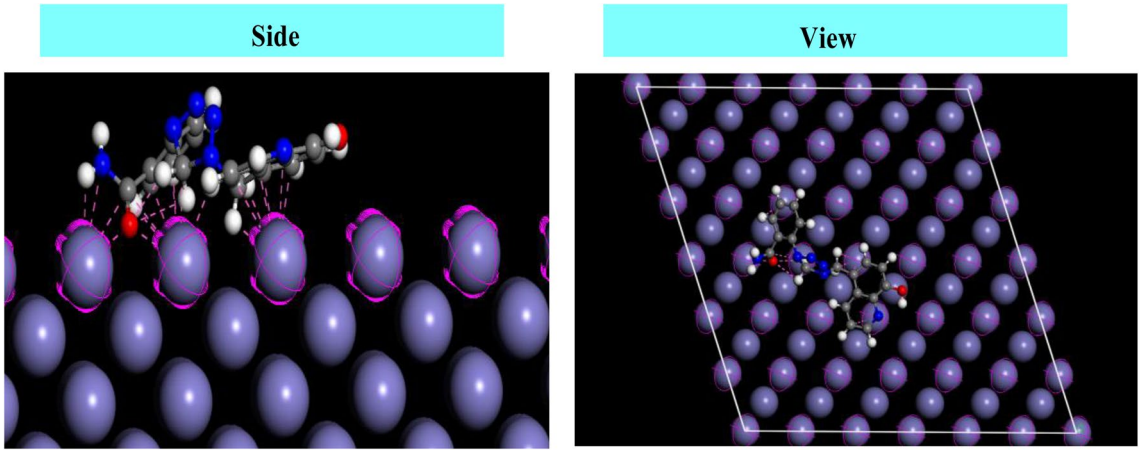

Fig. 16 Side and top views of stable adsorption configurations for QTB on Fe(110)

Table 9 Outputs and descriptors calculated by Monte Carlo simulation for adsorption of QTB on Fe(110) surface (in kcal/mol)

Systems	Total energy	Adsorption energy	Rigid adsorption energy	Deformation energy	dEad/dNi: inhibitor
Fe(110) + QTB	99.999	− 1376.030	− 65.713	− 1310.317	− 1376.030

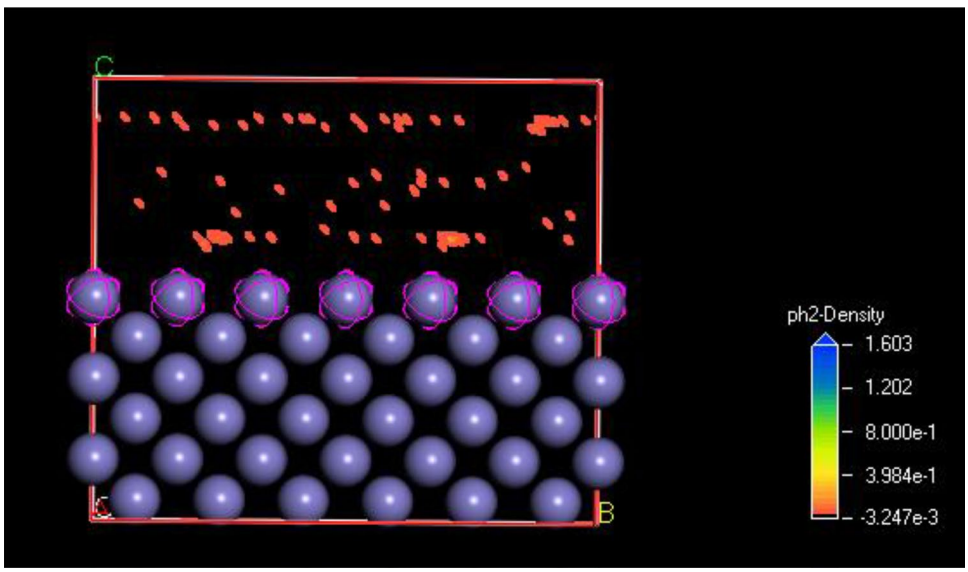

Fig. 17 Iso-surface density field for the Fe(110)/(QTB) interface

concentration of QTB while decreases with rise temperature. The adsorption of QTB on the steel surface obeys to the Langmuir's adsorption isotherm. The correlation between the quantum chemical parameters and inhibition efficiencies of QTB was investigated using DFT calculations. The inhibition efficiencies of the inhibitor are closely related to the quantum chemical parameters E_{HOMO}, E_{LUMO}, dipole moment,… The fact that inhibition efficiency is increased with an increase in E_{HOMO} value and with a decrease in E_{LUMO} value has been established herein. The Monte Carlo simulation were found to be in good agreement with the experimental. The adsorption energy obtained for the molecule studied reaches -51.0 kcal mol^{-1}) this value is considered as the suitable adsorption energy on the metal surface of Fe(110).

References

1. Bahrami MJ, Hosseini SMA, Pilvar P (2010) Experimental and theoretical investigation of organic compounds as inhibitors for mild steel corrosion in sulfuric acid medium. Corros Sci 52:2793–2803
2. Schmitt G (1984) Application of inhibitors for acid media: report prepared for the European federation of corrosion working party on inhibitors. Br Corros J 19:165–176
3. Zarrok H, Saddik R, Oudda H, Hammouti B, El Midaoui A, Zarrouk A, Benchat N, Ebn Touhami M (2011) 5-(2-chlorobenzyl)-2, 6-dimethylpyridazin-3-one: an efficientInhibitor of C38 steel corrosion in hydrochloric acid. Der Pharm Chem 3:272–282
4. Abboud Y, Abourriche A, Saffaj T, Berrada M, Charrouf M, Bennamara A, Hannache H (2009) A novel azo dye, 8-quinolinol-5-azoantipyrine as corrosion inhibitor for mild steel in acidic media. Desalination 237:175–189
5. Mernari B, El Attari H, Traisnel M, Bentiss F, Lagrenee M (1998) Inhibiting effects of 3, 5-bis (n-pyridyl)-4-amino-1, 2, 4-triazoles on the corrosion for mild steel in 1 M HCl medium. Corros Sci 40:391–399
6. Obot IB, Ebenso EE, Kabanda MM (2013) Metronidazole as environmentally safe corrosion inhibitor for mild steel in 0.5 M HCl: experimental and theoretical investigation. J Environ Chem Eng 1:431–439
7. El-Maksoud SAA (2003) The influence of some Arylazobenzoyl acetonitrile derivatives on the behaviour of carbon steel in acidic media. Appl Surf Sci 206:129–136
8. Kertit S, Hammouti B (1996) Corrosion inhibition of iron in 1 M HCl by 1-phenyl-5-mercapto-1, 2, 3, 4-tetrazole. Appl Surf Sci 93:59–66
9. Hassan HH, Abdelghani E, Amin MA (2007) Inhibition of mild steel corrosion in hydrochloric acid solution by triazole derivatives: part I. Polarization and EIS studies. Electrochim Acta 52:6359–6366
10. Watson AA, Fleet GW, Asano N, Molyneux RJ, Nash RJ (2001) Polyhydroxylated alkaloids—natural occurrence and therapeutic applications. Phytochemistry 56:265–295
11. Atwell GJ, Baguley BC, Denny WA (1998) Potential antitumor agents. 57. 2-Phenylquinoline-8-carboxamides as minimal DNA-intercalating antitumor agents with in vivo solid tumor activity. J Med Chem 32:396–401
12. Lukovits I, Kalman E, Zucchi F (2001) Corrosion inhibitors—correlation between electronic structure and efficiency. Corrosion 57:3–8
13. Frisch MJ, Trucks GW, Schlegel HB et al (2008) Gaussian 03, Revision C.02
14. El Faydy M, Galai M, Touhami ME, Obot IB, Lakhrissi B, Zarrouk A (2017) Anticorrosion potential of some 5-amino-8-hydroxyquinolines derivatives on carbon steel in hydrochloric acid solution: gravimetric, electrochemical, surface morphological, UV–visible, DFT and Monte Carlo simulations. J Mol Liq 248:1014–1027
15. Sun H (1998) COMPASS: an ab initio force-field optimized for condensed-phase applications overview with details on alkane and benzene compounds. J Phys Chem B 102:7338–7364
16. Cao C (1996) On electrochemical techniques for interface inhibitor research. Corros Sci 38:2073–2082
17. Moradi M, Duan J, Du X (2013) Investigation of the effect of 4,5-dichloro-2-n-octyl-4-isothiazolin-3-one inhibition on the corrosion of carbon steel in *Bacillus* sp. inoculated artificial seawater. Corros Sci 69:338–345
18. El Faydy M, Touir R, Ebn Touhami M, Zarrouk A, Jama C, Lakhrissi B, Olasunkanmi LO, Ebenso EE, Bentiss F (2018) Corrosion inhibition performance of newly synthesized 5-alkoxymethyl-8-hydroxyquinoline derivatives for carbon steel in 1 M HCl solution: experimental, DFT and Monte Carlo simulation studies. Phys Chem Chem Phys 20:20167–20187
19. Prabhu RA, Venkatesha TV, Shanbhag AV, Kulkarni GM, Kalkhambkar RG (2008) Inhibition effects of some Schiff's bases on the corrosion of mild steel in hydrochloric acid solution. Corros Sci 50:3356–3362
20. Tang Y, Yang X, Yang W, Chen Y, Wan R (2010) Experimental and molecular dynamics studies on corrosion inhibition of mild steel by 2-amino-5-phenyl1,3,4-thiadiazole. Corros Sci 52:242–249
21. Tebbji K, Faska N, Tounsi A, Oudda H, Benkaddour M, Hammouti B (2007) The effect of some lactones as inhibitors for the corrosion of mild steel in 1 M hydrochloric acid. Mater Chem Phys 106:260–267
22. Bentiss F, Lebrini M, Lagreneé M (2005) Thermodynamic characterization of metal dissolution and inhibitor adsorption processes in mild steel/2, 5-bis (n-thienyl)-1, 3, 4-thiadiazoles/hydrochloric acid system. Corros Sci 47:2915–2931
23. Riggs OL, Hurd RM (1967) Temperature coefficient of corrosion inhibition. Corrosion 33:252–260
24. Liu R, Qiao Y, Yan M, Fu Y (2012) Effects of rare earth elements on the characteristics of low temperature plasma nitrocarburized martensitic stainless steel. J Mater Sci Technol 28:1046–1052
25. Durnie W, Marco R, Jefferson A, Kinsella B (1999) Development of a structure-activity relationship for oil field corrosion inhibitors. Electrochem Soc 146:1751–1756
26. Hosseini SMA, Salari M, Ghasemi M, Abaszadeh M (2009) Enaminone compounds as corrosion inhibitors for austenitic stainless steel in sulphuric acid solution. Z Phys Chem 223:769–779
27. Tayebi H, Bourazmi H, Himmi B, El Assyry A, Ramli Y, Zarrouk A, Geunbour A, Hammouti B (2014) Combined electrochemical and quantum chemical study of new quinoxaline derivative as corrosion inhibitor for carbon steel in acidic media. Der Pharm Chem 6(5):220–234
28. Tayebi H, Bourazmi H, Himmi B, El Assyry A, Ramli Y, Zarrouk A, Geunbour A, Hammouti B, Ebenso EE (2014) An electrochemical and theoretical evaluation of new quinoline derivative as a corrosion inhibitor for carbon steel in HCL solutions. Der Pharm Lett 6(6):20–34
29. Zarrouk A, Zarrok H, Salghi R, Touir R, Hammouti B, Benchat N, Afrine LL, Hannache H, El Hezzat M, Bouachrine M

(2013) Electrochemical impedance spectroscopy weight loss and quantum chemical study of new pyridazine derivative as inhibitor corrosion of copper in nitric acid. J Chem Pharm Res 5(12):1482–1491
30. Zarrok H, Salghi R, Zarrouk A, Hammouti B, Oudda H, Bazzi L, Bammou L, Al Deyab SS (2012) Investigation of the inhibition effect of N-1-Naphthylethylenediamine dihydrochloride monomethanolate on the C38 steel corrosion in 0.5 M H_2SO_4. Der Pharma Chem 4(1):407–416
31. Tazouti A, Galai M, Touir R, Touhami ME, Zarrouk A, Ramli Y, Saraçoğlu M, Kaya S, Kandemirli F, Kaya C (2016) Experimental and theoretical studies for mild steel corrosion inhibition in 1.0 M HCl by three new quinoxalinone derivatives. J Mol Liq 222:239–252
32. Obot IB, Macdonald DD, Gasem ZM (2015) Density functional theory (DFT) as a powerful tool for designing new organic corrosion inhibitors. Part 1: an overview. Corros Sci 99:1–30
33. Frisch MJ et al (2009) Gaussian 09, revision D 01
34. Lee C, Yang W, Parr RG (1988) Development of the Colle-Salvetti correlation-energy formula into a functional of the electron density. Phys Rev B 37:785–789
35. Zarrouk A, Zarrok H, Ramli Y, Bouachrine M, Hammouti B, Sahibed-dine A, Bentiss F (2016) Inhibitive properties, adsorption and theoretical study of 3,7-dimethyl-1-(prop-2-yn-1-yl) quinoxalin-2(1H)-one as efficient corrosion inhibitor for carbon steel in hydrochloric acid solution. J Mol Liq 222:239–252
36. Abdel-Gaber AM, Abd-El-Nabey BA, Sidahmed IM, El-Zayady AM, Saadawy M (2006) Inhibitive action of some plant extracts on the corrosion of steel in acidic media. Corros Sci 48:2765–2779
37. El Azzouzi M, Aouniti A, Tighadouin S, Elmsellem H, Radi S, Hammouti B, El Assyry A, Bentiss F, Zarrouk A (2016) Some hydrazine derivatives as corrosion inhibitors for mild steel in 1.0 M HCl: weight loss, electrochemichal, SEM and theoretical studies. J Mol Liq 221:633–641
38. El Hezzat M, Assouag M, Zarrok H, Benzekri Z, El Assyry A, Boukhris S, Souizi A, Galai M, Touir R, Ebn Touhami M, Oudda H, Zarrouk A (2015) Correlated DFT and electrochemical study on inhibition behavior of ethyl 6-amino-5-cyano-2-methyl-4-(p-tolyl)-4H-pyran-3-carboxylate for the corrosion of mild steel in HCl. Der Pharm Chem 7(10):77–88
39. Zhang K, Xu B, Yang W, Yin X, Liu Y (2015) Halogen-substituted imidazoline derivatives as corrosion inhibitors for mild steel in hydrochloric acid solution. Corros Sci 90:284–295
40. Kaya S, Guo L, Kaya C, Tuzun B, Obot IB, Touir R, Islam N (2016) Quantum chemical and molecular dynamic simulation studies for the prediction of inhibition efficiencies of some piperidine derivatives on the corrosion of iron. J Taiwan Inst Chem Eng 65:522–529
41. ELouadi Y, Abrigach F, Bouyanzer A, Touzani R, Riant O, ElMahi B, El Assyry A, Radi S, Zarrouk A, Hammouti B (2015) Corrosion inhibition of mild steel by new N-heterocyclic compound in 1 M HCl: experimental and computational study. Der Pharm Chem 7(8):265–275
42. Olasunkanmi LO, Kabanda MM, Ebenso EE (2016) Quinoxaline derivatives as corrosion inhibitors for mild steel in hydrochloric acid medium: electrochemical and quantum chemical studies. Phys E Low-Dimens Syst Nanostruct 76:109–126
43. Ahamad I, Prasad R, Quraishi MA (2010) Inhibition of mild steel corrosion in acid solution by Pheniramine drug: experimental and theoretical study. Corros Sci 52:3033–3041
44. Sebastian SHR Sr., Attia MI, Almutairi MS, El-Emam AA, Panicker CY, van Alsenoy C (2014) FT-IR, FT-Raman, molecular structure, first order hyperpolarizability, HOMO and LUMO analysis, MEP and NBO analysis of 3-(adamantan-1-yl)-4-(prop-2-en-1-yl)-1H-1, 2, 4-triazole-5 (4H)-thione, a potential bioactive agent. Spectrochim Acta A Mol Biomol Spectrosc 132:295–304
45. Panicker CY, Varghese HT, Manjula PS, Sarojini BK, Narayana B, War JA, Srivastava SK, van Alsenoy C, Al-Saadi AA (2015) FT-IR, HOMO–LUMO, NBO, MEP analysis and molecular docking study of 3-Methyl-4-{(E)-[4-(methylsulfanyl)-benzylidene] amino} 1H-1, 2, 4-triazole-5 (4H)-thione. Spectrochim Acta A Mol Biomol Spectrosc 151:198–207
46. Kaya S, Kaya C, Guo L, Kandemirli F, Tüzün B, Uğurlu İ, Madkour LH, Saraçoğlu M (2016) Quantum chemical and molecular dynamics simulation studies on inhibition performances of some thiazole and thiadiazole derivatives against corrosion of iron. J Mol Liq 219:497–504
47. Saha SK, Murmu M, Murmu NC, Banerjee P (2016) Evaluating electronic structure of quinazolinone and pyrimidinone molecules for its corrosion inhibition effectiveness on target specific mild steel in the acidic medium: a combined DFT and MD simulation study. J Mol Liq 224:629–638
48. Eddy NO, Momoh-Yahaya H, Oguzie EE (2015) Theoretical and experimental studies on the corrosion inhibition potentials of some purines for aluminum in 0.1 M HCl. J Adv Res 6:203–217
49. Shahraki M, Dehdab M, Elmi S (2016) Theoretical studies on the corrosion inhibition performance of three amine derivatives on carbon steel: molecular dynamics simulation and density functional theory approaches. J Taiwan Inst Chem Eng 62:313–321
50. Lewis GN (1923) Valence and the structure of atoms and molecules. Chemical Catalog Company Inc, New York
51. Kaya S, Banerjee P, Saha SK, Tüzün B, Kaya C (2016) Theoretical evaluation of some benzotriazole and phospono derivatives asaluminum corrosion inhibitors: DFT and molecular dynamics simulation approaches. RSC Adv 6:74550–74559